Conformational Analysis, Barriers to Internal Rotation, ab Initio Calculations, and Vibrational Assignment of 4-Fluoro-1-butyne

Gamil A. Guirgis,[†] Xiaodong Zhu,[‡] Stephen Bell,[§] and James R. Durig*

Department of Chemistry, University of Missouri—Kansas City, Kansas City, Missouri 64110-2499

Received: June 16, 2000; In Final Form: September 26, 2000

The infrared spectra (3400−300 cm^{-1}) of gaseous, xenon and krypton solutions, and solid state and the Raman spectra (3400−10 cm^{-1}) of the liquid and solid states have been recorded for 4-fluoro-1-butyne, CH_2FCH_2-C≡CH. These data have been interpreted to show that the molecule exists in the anti conformation (the C−F bond is trans to the C≡C bond) and the gauche forms in the vapor and liquid, but only the gauche conformer is present in the solid. From variable-temperature infrared studies of xenon and krypton solutions, the anti conformation has been determined to be more stable than the gauche form by 215 ± 22 cm^{-1} (2.57 ± 0.26 kJ/mol) and 170 ± 17 cm^{-1} (2.04 ± 0.2 kJ/mol), respectively. The asymmetric torsional fundamentals have been observed at 109.4 and 116.6 cm^{-1} for the more stable anti and the high-energy gauche conformers, respectively. From these data the asymmetric torsional potential function governing the internal rotation about the C−CH_2F bond has been determined and the potential parameters are $V_1 = 438 \pm 14$, $V_2 = -157 \pm 12$, $V_3 = 1137 \pm 5$, and $V_4 = 17 \pm 6$ cm^{-1}. This potential function is consistent with the anti to gauche and gauche to gauche barriers of 1142 and 1364 cm^{-1}, respectively, and the dihedral angle FCCC for the gauche conformer of 64°. These data are compared to the corresponding quantities obtained from ab initio calculations, which predict the anti conformer to be the more stable form. Vibrational assignments for the 24 normal modes for both the anti and gauche conformers are proposed. These experimental and theoretical results are compared to the corresponding quantities of some similar molecules.

Introduction

Rotational isomerism of molecules with the general formula FCH_2–CH_2X (where X= F, Cl, Br, or I) has been the subject of numerous investigations.[1−12] It is interesting that the gauche conformer of 1,2-difluoroethane, FCH_2CH_2F, is more stable than the anti conformer in the vapor phase, whereas in the corresponding 1-fluoro-2-chloro-, 1-fluoro-2-bromo-, and 1-fluoro-2-iodoethane molecules,[13−16] the reverse conformational equilibrium is found. To obtain more information on the unusual stability of *gauche*-1,2-difluoroethane, we investigated the conformational stability of 1-fluoropropane[17] and found that the gauche rotamer is the more stable form in both krypton and xenon solutions with enthalpy differences of 104 ± 6 cm^{-1} (1.24 ± 0.07 kJ/mol) and 99 ± 5 cm^{-1} (1.16 ± 0.06 kJ/mol), respectively. Therefore, for molecules with the general formula FCH_2CH_2X there appear to be at least two factors that influence the relative stability of the gauche and anti conformers: the size and the electronegativity of the X substituent. If the conformational stability were influenced only by the size, then 1-fluoro-2-chloroethane and 1-fluoropropane would be expected to have the same conformational stability since the methyl group and the chlorine atom are approximately the same size. Since these two molecules have the two different conformers as the stable forms, it is clear that size is not a dominant factor in determining the conformer stability in these molecules.

As a continuation of these studies we have investigated the conformational stability of 4-fluoro-1-butyne, FCH_2CH_2CCH, with X = C≡CH. There have been no previous spectroscopic studies reported for this molecule. Therefore, we have recorded the Raman spectra of the liquid and solid along with infrared spectra of the gas, xenon and krypton solutions with variable temperatures, and the solid. We have also carried out ab initio calculations employing the 6-31G(d) basis set at the level of restricted Hartree−Fock (RHF) and 6-31G(d) with Moller−Plesset to the second order (MP2) to obtain equilibrium geometries, force constants, vibrational frequencies, infrared and Raman intensities, and conformational stabilities. Structural parameters and conformational stabilities have also been obtained from the larger basis sets of 6-311+G(d,p) and 6-311+G(2df,2p). The results of this spectroscopic and theoretical study are reported herein.

Experimental Section

The sample of 4-fluoro-1-butyne was prepared by the reaction of 1-butyn-4-ol with diethylaminosulfur trifluoride in diglyme at −50 °C for 2 h. The sample was frozen with liquid nitrogen and degassed. It was then warmed to room temperature and the volatile material was collected and washed, first with 5% sodium bicarbonate and then with distilled water. The sample was finally purified on a low-temperature and low-pressure sublimation column. The purity of the sample was checked by NMR and mass spectroscopy.

The Raman spectra were recorded on a SPEX model 1403 spectrometer equipped with a Spectra-Physics model 164 argon

* Corresponding author: phone 01 816-235-6038; fax 01 816-235-5502; e-mail durigj@umkc.edu.

[†] Permanent address: Organic Products Division, Analytical R/D Department, Bayer Corp., Bushy Park Plant, Charleston SC 29411.

[‡] Taken in part from the dissertation of X.Z., which will be submitted to the Department of Chemistry in partial fulfillment of the Ph.D. degree.

[§] Permanent Address: Department of Chemistry, The University of Dundee, Dundee DD1 4HN, Scotland, U.K.

10.1021/jp0021796 CCC: $20.00
Published on Web 12/22/2000

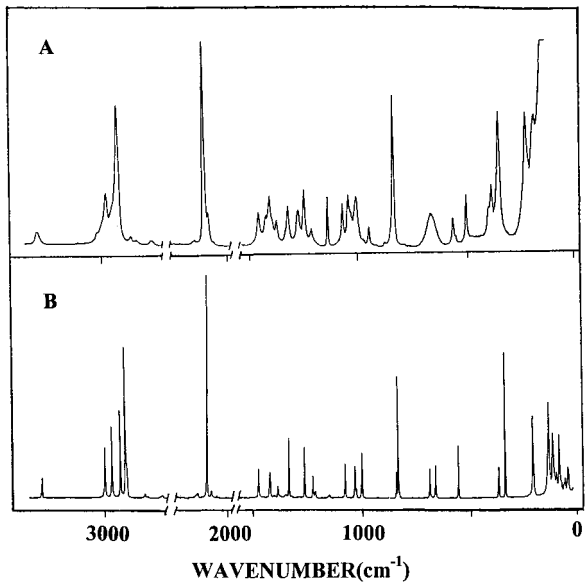

Figure 1. Raman spectra of 4-fluoro-1-butyne: (A) liquid; (B) solid.

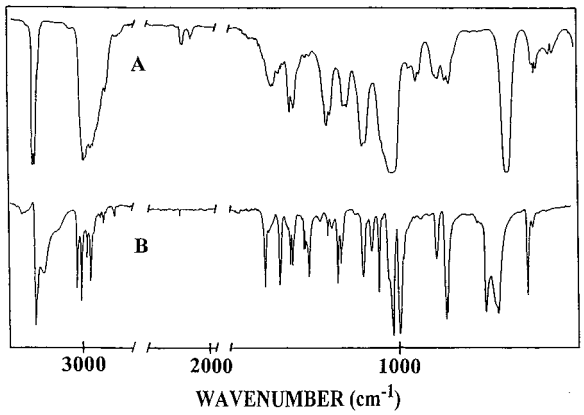

Figure 2. Infrared spectra of (A) gaseous and (B) solid 4-fluoro-1-butyne.

ion laser operating on the 514.5 nm line. The laser power used was 0.5 W for the liquid and the solid with a spectral bandpass of 3 cm^{-1}. The spectrum of the liquid was recorded with the sample sealed in a Pyrex glass capillary. Depolarization measurements were obtained for the liquid sample with a standard Ednalite 35 mm camera polarizer with 38 mm of free aperture affixed to the SPEX instrument. Depolarization ratio measurements were checked by measuring the state of polarization of the Raman bands of carbon tetrachloride immediately before depolarization measurements were made on the liquid sample. The Raman frequencies are expected to be accurate to ± 2 cm^{-1} and typical spectra are shown in Figure 1.

The midinfrared spectra (Figure 2) of the gas and solid were recorded on a Perkin-Elmer model 2000 Fourier transform spectrometer equipped with a Ge/CsI beam splitter and DTGS detector. Atmospheric water vapor was removed from the spectrometer housing by purging with dry nitrogen. The spectrum of the gas was obtained with the sample contained in a 10 cm cell. The spectrum of the solid was obtained by condensing the sample on a CsI substrate held at the temperature of boiling liquid nitrogen, housed in a vacuum cell fitted with CsI windows. The sample was condensed as an amorphous solid and repeatedly annealed until no further changes were observed in the spectra.

The midinfrared spectrum of the sample dissolved in liquified xenon (Figure 3) was recorded as a function of temperature on a Bruker model IFS Fourier transform spectrometer equipped

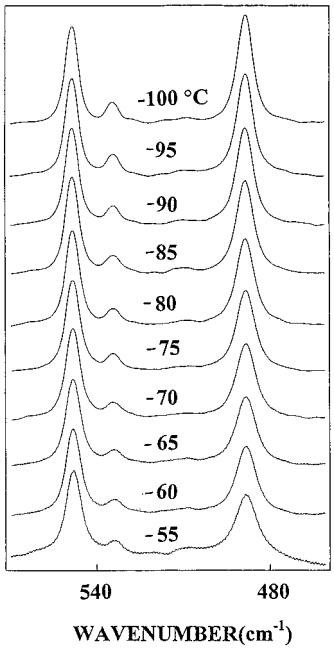

Figure 3. Temperature-dependent infrared spectra (460−570 cm^{-1}) of 4-fluoro-1-butyne in liquid xenon.

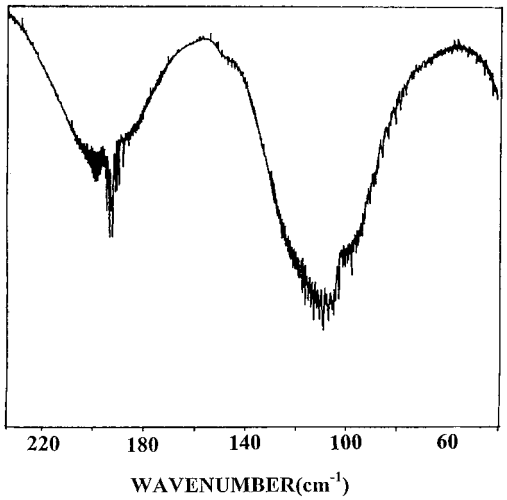

Figure 4. Far-infrared spectrum (40−240 cm^{-1}) of gaseous 4-fluoro-1-butyne.

with a globar source, a Ge/KBr beam splitter and a DTGS detector. For all spectra, 100 interferograms were collected at 1.0 cm^{-1} resolution, averaged, and transformed with a boxcar truncation function. For these studies a specially designed cryostat cell was used. It consists of a copper cell with a path length of 4 cm with wedged silicon windows sealed to the cell with an indium gasket. The cell was cooled by boiling liquid nitrogen and the temperature was monitored with two Pt thermoresistors. The complete cell was connected to a pressure manifold, allowing the filling and evacuation of the cell. After the cell has cooled to the desired temperature, a small amount of the compound was condensed into the cell. Next, the pressure manifold and the cell were pressurized with the noble gas, which immediately started to condense in the cell, allowing the compound to dissolve.

The far-infrared spectra of gaseous 4-fluoro-1-butyne (Figures 4−6) were recorded on a Nicolet model 200 SXV Fourier transform spectrometer equipped with a vacuum bench, 6.25 and 12.5 μm Mylar beam splitters, and a liquid helium-cooled Si bolometer. The spectrum was obtained with an effective

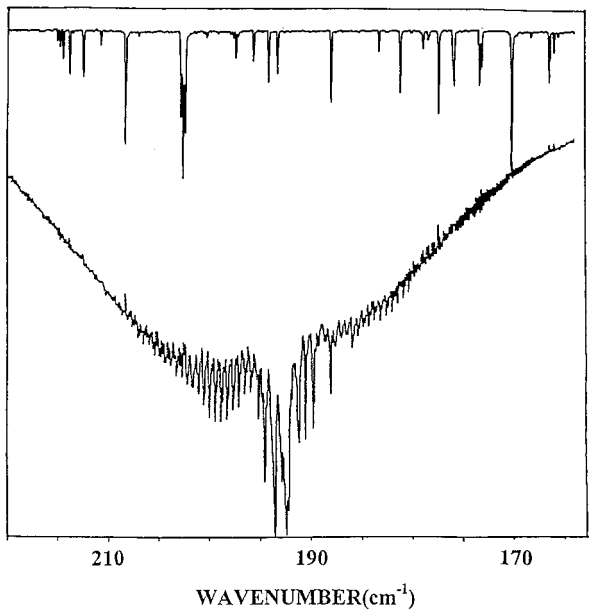

Figure 5. Far-infrared spectrum (162−220 cm^{-1}) of gaseous 4-fluoro-1-butyne. The top spectrum is that of water vapor.

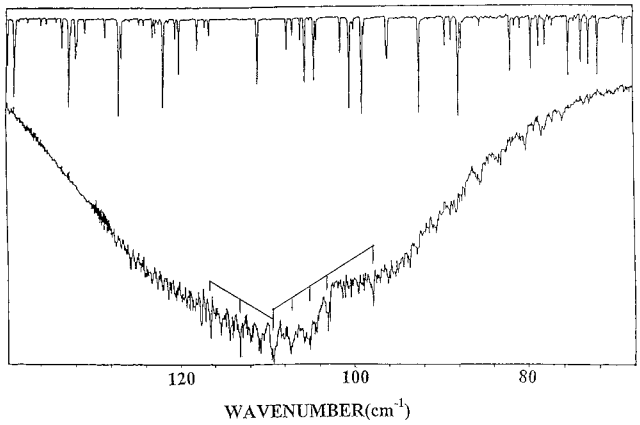

Figure 6. Far-infrared spectrum (68−140 cm^{-1}) of gaseous 4-fluoro-1-butyne. The top spectrum is that of water vapor.

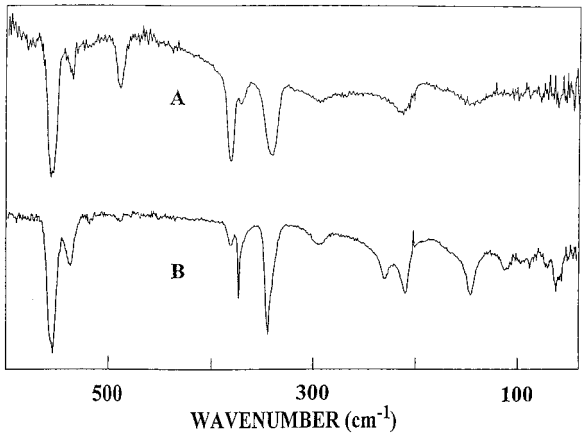

Figure 7. Far-infrared spectra of (A) amorphous and (B) annealed solid 4-fluoro-1-butyne.

resolution of 0.10 cm^{-1} from the sample contained in a 1 m folded path cell equipped with mirrors coated with gold and fitted with polyethylene windows. The spectrum of the crystalline solid (Figure 7) was obtained with a Perkin-Elmer model 2000 infrared Fourier transform spectrometer equipped with a metal grid beam splitter and a DTGS detector. The sample was deposited on a Si substrate held at 77 K with boiling liquid nitrogen, which was contained in a cryostat cell equipped with polyethylene windows. All of the bands of significant intensity observed in the infrared and Raman spectra with their proposed assignments are listed in Table 1S in the Supporting Information.

Ab Initio Calculations

Quantum chemical calculations were performed with the Gaussian 94 program[18] using Gaussian-type basis functions. The energy minima with respect to nuclear coordinates were obtained by simultaneous relaxation of the geometry parameters by the gradient method of Pulay.[19] The structural optimizations for the anti and gauche conformers were carried out with initial parameters taken from those obtained from the ab initio MP2/6-31G(d) calculations of 1-butyne[20] and 1-fluoropropane.[17] The structural parameters as determined by different methods for the anti and gauche conformers of 4-fluoro-1-butyne are listed in Tables 1 and 2, respectively.

The energies obtained by quantum chemical calculations of the anti and gauche conformers and the two intermediate maxima are given in Table 3. The anti conformer is the more stable form in every case, with the gauche conformer having higher energy by 290 cm^{-1} than the anti form from the MP2/6-31G(d) calculation. The lowest estimate of this energy difference is 245 cm^{-1}, which was obtained from the MP2/6-311+(d,p) calculation.

The force fields in Cartesian coordinates were obtained by the Gaussian 94 program[18] from the MP2/6-31G(d) calculation. Internal coordinates (Figure 8) were used to calculate the G and B matrixes from the structural parameters given in Tables 1 and 2. By use of the B matrix,[21] the force fields in Cartesian coordinates were then converted to force fields in internal coordinates, and the pure ab initio vibrational frequencies were reproduced. The force constants for the two conformers can be obtained from the authors. Subsequently, scaling factors of 0.88 for CH stretches, 0.9 for all other stretches and bends except for the C≡C−H and C−C≡C bends, with 1.3 and 1.0 for the torsional coordinate and C≡C stretch along with the geometric average of the scaling factors for interaction force constants were used to obtain the fixed scaled force field and resultant wavenumbers (Tables 4 and 5). The set of symmetry coordinates is given in Table 2S in the Supporting Information, and they were used to determine the corresponding potential energy distribution (PED). The calculated infrared intensities, Raman activities, depolarization ratios, and PED are also given in Tables 4 and 5.

Infrared spectra were calculated on the basis of the dipole moment derivatives with respect to the Cartesian coordinates. The derivatives were taken from the ab initio calculations at the MP2/6-31G(d) level and transformed to normal coordinates by

$$\left(\frac{\partial \mu_u}{\partial Q_i}\right) = \sum_j \left(\frac{\partial \mu_u}{\partial X_j}\right) L_{ij}$$

where Q_i is the ith normal coordinate, X_j is the jth Cartesian displacement coordinate, and L_{ij} is the transformation matrix between Cartesian displacement coordinates and normal coordinates. The infrared intensities were then calculated by

$$I_i = \frac{N\pi}{3c^2}\left[\left(\frac{\partial \mu_x}{\partial Q_i}\right)^2 + \left(\frac{\mu_y}{\partial Q_i}\right)^2 + \left(\frac{\partial \mu_z}{\partial Q_i}\right)^2\right]$$

The predicted infrared spectra of the anti and the gauche conformers are shown in Figure 9. The combination of the two

TABLE 1: Geometrical Parameters[a] for *anti* 4-Fluoro-1-butyne Obtained from ab Initio and Hybrid DFT Calculations

parameter	internal coordinate	RHF 6-31G	MP2 6-31G(d)	B3LYP 6-31G(d)	MP2/6-311+G(d,p)
C_1C_2	S	1.1947	1.2202	1.2073	1.2181
C_2C_3	T	1.4653	1.4628	1.4614	1.4613
C_3C_4	U	1.5204	1.5220	1.5314	1.5218
C_4F	V	1.4205	1.3976	1.3894	1.3924
$C_1C_2C_3$	x	179.21	177.48	178.12	180.0[b]
$C_2C_3C_4$	q	111.67	111.10	112.01	110.79
C_3C_4F	c	107.63	108.33	108.66	109.01
$C_2C_3C_4F$	t	180.00	180.00	180.00	180.0[b]
C_1H_1	r_1	1.0530	1.0666	1.0663	1.0644
$C_2C_1H_1$	z	180.16	181.40	180.74	180.0[b]
$C_3H_{2,3}$	$r_{2,3}$	1.0837	1.0951	1.0977	1.0941
$C_4C_3H_{2,3}$	$\gamma_{2,3}$	108.91	108.64	108.52	109.04
$C_2C_4C_3H_2$[c]	ϕ_2	121.80	121.86	122.20	120.70
$C_4H_{4,5}$	$r_{4,5}$	1.0772	1.0933	1.0957	1.0920
$C_3C_4H_{4,5}$	$\beta_{4,5}$	112.08	111.13	110.86	110.99
$FC_3C_4H_4$[b]	ϕ_4	117.78	119.03	119.44	118.85
rotational constants					
A		27 603.1	26 693.3	27 015.1	27 191.6
B		2225.3	2238.5	2229.3	2231.4
C		2112.7	2120.2	2113.9	2117.2
$\lvert\mu_a\rvert$				1.099	1.594
$\lvert\mu_b\rvert$				0.379	0.481
$\lvert\mu_c\rvert$				0.000	0.000
$\lvert\mu_t\rvert$				1.1626	1.665
$-(E + 253)$				2.192 443 2	1.681 586 4

[a] Bond lengths are given in angstroms, bond angles in degrees, rotational constants in megaherytz, dipole moments in debyes, and total energy in hartrees. [b] Held at 180.0° for convergence. [c] Dihedral angle of symmetrically equivalent H is negative value.

TABLE 2: Geometrical Parameters[a] for *gauche* 4-Fluoro-1-butyne Obtained from ab Initio and Hybrid DFT Calculations

parameter	internal coordinate	RHF 6-31G	MP2 6-31G(d)	B3LYP 6-31G(d)	MP2/6-311+G (d,p)
C_1C_2	S	1.1942	1.2199	1.2069	1.2178
C_2C_3	T	1.4648	1.4632	1.4625	1.4617
C_3C_4	U	1.5177	1.5195	1.5295	1.5193
C_4F	V	1.4182	1.3944	1.3863	1.3897
$C_1C_2C_3$	x	180.02	180.27	179.61	180.0[b]
$C_2C_3C_4$	q	113.48	112.46	113.58	112.56
C_3C_4F	c	109.28	109.21	109.98	109.64
$C_2C_3C_4F$	t	65.61	62.66	64.10	64.66
C_1H_1	r_1	1.0529	1.0664	1.0662	1.0644
$C_2C_1H_1$	z	179.74	178.97	179.87	180.0[b]
C_3H_2	r_2	1.0859	1.0973	1.0994	1.0944
$C_2C_3H_2$	γ_2	108.33	108.65	108.12	110.00
$C_4C_2C_3H_2$	ϕ_2	121.79	122.10	122.31	121.56
C_3H_3	r_3	1.0839	1.0956	1.098	1.0963
$C_2C_3H_3$	γ_3	108.72	108.47	108.37	109.75
$C_4C_2C_3H_3$	ϕ_3	−122.29	−121.90	−122.58	−120.48
C_4H_4	r_4	1.0788	1.095	1.0972	1.0922
$C_3C_4H_4$	β_4	111.01	110.60	109.86	110.45
$C_2C_3C_4H_4$	ϕ_4	117.64	118.92	119.29	119.07
C_4H_5	r_5	1.0771	1.0935	1.0960	1.0933
$C_3C_4H_5$	β_5	112.12	111.12	110.87	111.11
$C_2C_3C_4H_5$	ϕ_5	−118.63	−119.27	−119.97	−119.14
rotational constants					
A		11 242.6	11 054.5	11 267.0	11 183.9
B		3108.4	3167.0	3100.5	3139.4
C		2634.5	2662.4	2626.8	2651.6
$\lvert\mu_a\rvert$				0.084	0.112
$\lvert\mu_b\rvert$				1.665	2.221
$\lvert\mu_c\rvert$				0.545	0.753
$\lvert\mu_t\rvert$				1.754	2.348
$-(E + 253)$				2.190 792 3	1.680 471

[a] Bond lengths are given in angstroms, bond angles in degrees, and rotational constants in megahertz. [b] Held at 180.0° for convergence.

spectra for the conformers with ΔH of 215 cm^{-1} between the more stable anti conformer and the less stable gauche conformer is shown in Figure 9. The ΔH value used was taken from the temperature-dependent measurements of the xenon solution performed in this study. The predicted infrared spectrum was very useful for identifying the bands due to the two conformers in the infrared spectrum of the sample dissolved in liquid xenon.

The predicted Raman spectra (Figure 10) for the two conformers of 4-fluoro-1-butyne and the room temperature mixture were calculated from scattering activities determined from the RHF/6-31G(d) ab initio calculations. The Gaussian-94 program[18] with the option of calculating the polarizability derivatives was used. The evaluation of Raman activity by using the analytical gradient methods has been developed[22,23] and the

TABLE 3: Ab Initio and Hybrid DFT Energies[a] and Energy Differences between Conformers for 4-Fluoro-1-butyne

		energy differences,[b] ΔE (cm^{-1})		
	energy, anti (H)	gauche (angle, deg)	cis	barrier (angle, deg)
RHF/6-31G	3.665 797 9	621 (65.61)	2608	1582 (116.10)
RHF/6-31G(d)[c]	3.743 525 8	444 (62.62)	2460	1563 (117.40)
MP2/6-31G(d)	4.420 689 7	290 (62.66)	2185	1554 (117.40)
MP2/6-311 +G(d,p)	4.681 586 4	245 (64.66)		
MP2/6-311 +G(2df,2p)[d]	4.719 805 1	274 (62.66)		
B3LYP/6-31G(d)	5.192 443 2	362 (62.66)	2089	1444 (117.60)

[a] Energies are given in hartrees. That of the anti conformer is given as $-(E + 250)$ H. Energy differences are given in reciprocal centimeters. Angles are given in degrees. All MP calculations are frozen core. Geometries are fully optimized unless indicated. [b] Differences are relative to the anti form, which is the lowest energy conformer. [c] At geometries of MP2/6-31G(d). [d] At geometries of B3LYP/6-31G(d).

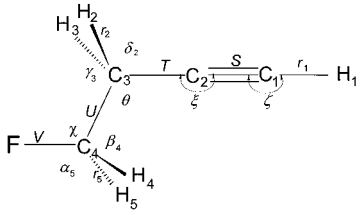

Figure 8. Internal coordinates of 4-fluoro-1-butyne.

activity S_j can be expressed as

$$S_j = g_j(45\alpha_j^2 + 7\beta_j^2)$$

where g_j is the degeneracy of the vibrational mode j, α_j is the derivative of the isotropic polarizability, and β_j is that of the anisotropic polarizability. The Raman scattering cross sections, $\partial\sigma/\partial\Omega$, which are proportional to the Raman intensities, can be calculated from the scattering activities and the predicted frequencies for each normal mode by use of the following relationship:[24,25]

$$\frac{\partial\sigma_j}{\partial\Omega} = \left(\frac{2^4\pi^4}{45}\right)\left(\frac{(\nu_0 - \nu_j)^4}{1 - \exp\left[\frac{-hc\nu_j}{kT}\right]}\right)\left(\frac{h}{8\pi^2 c\nu_j}\right)S_j$$

where ν_0 is the exciting frequency, ν_j is the vibrational frequency of the jth normal mode, h, c, and k are the universal constants, and S_j is the corresponding Raman scattering activity. To obtain the polarized Raman scattering cross section, the polarizabilities are incorporated in S_j by $S_j\ (1 - \rho_j)/(1 + \rho_j)$, where ρ_j is the depolarization ratio of the jth normal mode. The Raman scattering cross section and calculated frequencies are used together with a Lorentzian line shape function to obtain the calculated spectrum. The predicted Raman spectra of the anti and the gauche conformers individually are shown in Figure 10, spectra D and C, respectively, along with the combination of the two spectra with ΔH of 215 cm^{-1} (Figure 10B). The agreement between the predicted spectrum (Figure 10B) and the observed one (Figure 10A) is not as good as usually found, possibly because the ΔH value may be significantly different in the liquid.

Vibrational Assignment

Since no spectroscopic studies have been reported for this molecule, we utilized the frequencies predicted from the ab initio calculations along with the relative intensities, Raman activities, group frequencies, and infrared band contours to provide a complete vibrational assignment for the normal modes. The anti conformer of 4-fluoro-1-butyne possesses C_s symmetry and the 24 fundamental vibrations are divided into 15A′ and 9A″ normal modes, all of which are infrared- and Raman-active. The A′ modes should give rise to polarized lines in the Raman spectra of the fluid phases, whereas the A″ modes will be depolarized. The symmetry plane of the molecule for the anti conformer contains the *a* and *b* principal axes and, therefore, the A, B, or A/B hybrid infrared band contours must be due to A′ modes, whereas the A″ fundamentals should have C-type band contours. For the gauche conformer with C_1 symmetry, the 24 normal modes should give rise to A/B/C infrared hybrid band contours and polarized Raman lines. The complete assignments of the normal modes of the anti and the gauche conformers are reported in Tables 4 and 5, respectively.

Carbon−Hydrogen Modes. For the anti conformer, a total of five carbon−hydrogen stretching modes are divided into 3A′ and 2A″ modes. The CH of the acetylenic group is observed as a strong, A-type band in the infrared spectrum of the gas at 3331 cm^{-1} for both conformers. There are two methylene groups in this molecule: one has a fluorine atom attached and is indicated as $*CH_2$, and the other is directly attached to the acetylenic group and is simply indicated as CH_2. The CH_2 stretching modes for these two groups are predicted from the ab initio calculations to be different, with the normal modes for the $*CH_2$ group having higher frequencies than those for the corresponding CH_2 modes. Therefore, the four carbon−hydrogen stretches for the $*CH_2$ and CH_2 groups are assigned as predicted by ab initio calculations with the antisymmetric stretches having the next higher frequencies after the acetylenic CH stretch at 3333 cm^{-1}. The four carbon−hydrogen bends (scissor, wag, twist, and rock) for both the $*CH_2$ and CH_2 groups are assigned according to the prediction obtained from the ab initio calculations. The acetylenic CH bends are predicted too high from the RHF/6-31G(d) calculations and much too low by the MP2/6-31G(d) calculations, so a scaling factor of 1.3 is needed with the latter calculations to obtain reasonable predicted frequencies for these modes, which are assigned at 643 and 639 cm^{-1}. It should be noted that the B3LYP/6-31G(d) calculations give excellent predictions for these modes.

Skeletal Modes. The C_3–C_4, C−F, and C_2–C_3 stretches are assigned at 1071, 1045, and 953 cm^{-1}, respectively, for the anti conformer, where these frequencies differ from the predicted ones by only 12, 0, and 3 cm^{-1}, respectively. The corresponding modes for the gauche conformer are assigned at 1049, 1019, and 838 cm^{-1}, respectively. The $C_2C_3C_4$, CCF, and C−C═C (out-of-plane) bends can confidently be assigned at 487, 386, and 334 cm^{-1}, respectively, for the anti conformer. For the gauche conformer, these modes are assigned at 548, 347, and 325 cm^{-1}, respectively.

In the far-infrared spectrum below 300 cm^{-1}, there are two strong bands around 193 and 110 cm^{-1}, both showing fine structure. The band at 193 cm^{-1} is evidently a C-type band of the gauche conformer from the contour of the rotational fine structure, which shows K-subbands with a spacing of approximately 0.57 cm^{-1} as expected for this conformer from the rotational constants in Table 2 and as shown in Figure 11. The frequency of the central peak is readily assigned from the MP2 calculated frequencies listed in Table 4 as ν_{15}, a skeletal bending mode. In addition to the K structure, there are a number of peaks to both higher and lower frequency, which are probably "hot band" sequences involving two low-frequency modes, i.e., the

TABLE 4: Vibrational Frequencies[a] of *anti*-4-Fluoro-1-butyne

	vib no.	approximate description	RHF 6-31G unscaled	MP2 6-31G(d) unscaled	B3LYP 6-31G(d) unscaled	MP2 6-31G(d) scaled[b]	obs (gas)	IR int[c]	Raman act.[c]	dp ratios	PED
A′	ν_1	≡CH stretch	3675.0	3521.8	3495.7	3312.7	3332	54.7	30.2	0.18	$96S_1$
	ν_2	*CH_2 symmetric stretch	3275.5	3131.3	3064.3	2937.4	2926	31.1	84.9	0.12	$96S_2$
	ν_3	CH_2 symmetric stretch	3216.5	3114.0	3045.4	2921.2	2915	3.9	139.3	0.07	$96S_3$
	ν_4	$C_1{\equiv}C_2$ stretch	2394.2	2171.3	2243.0	2151.0	2139	0.01	85.7	0.29	$82S_4$, $14S_{11}$
	ν_5	*CH_2 scissors	1684.9	1588.6	1552.1	1507.8	1478	0.4	8.2	0.73	$98S_5$
	ν_6	CH_2 scissors	1645.0	1545.9	1509.4	1466.8	1457	4.3	21.1	0.71	$98S_6$
	ν_7	*CH_2 wag	1562.3	1473.5	1449.9	1398.4	1394	17.3	3.5	0.49	$79S_7$, $15S_8$
	ν_8	CH_2 wag	1466.5	1337.7	1326.9	1272.2	1266	1.9	5.9	0.54	$72S_8$, $19S_7$
	ν_9	C_3–C_4 stretch	1155.8	1106.4	1083.3	1059.2	1048	35.7	13.7	0.40	$71S_9$, $14S_{10}$
	ν_{10}	CF stretch	1102.9	1096.5	1057.4	1044.5	1036	73.3	10.3	0.39	$79S_{10}$
	ν_{11}	C_2–C_3 stretch	1028.9	988.9	979.3	949.9	953	5.5	2.4	0.14	$68S_{11}$, $11S_4$
	ν_{12}	C≡C−H bend ip	915.4	563.8	637.5	637.6	643	54.9	5.2	0.72	$91S_{12}$
	ν_{13}	$C_2C_3C_4$ bend	564.6	477.6	506.9	485.3	487	2.0	5.6	0.44	$36S_{13}$, $13S_{15}$, $12S_9$, $11S_{14}$
	ν_{14}	CCF bend	405.0	367.3	381.7	373.5	386	8.1	4.8	0.61	$64S_{14}$, $20S_{15}$
	ν_{15}	C−C≡C bend ip	184.3	138.7	158.8	148.2	149	0.8	6.9	0.74	$61S_{15}$, $36S_{13}$
A″	ν_{16}	*CH_2 antisymmetric stretch	3343.1	3199.6	3117.4	3001.5	2988	35.5	38.6	0.75	$90S_{16}$
	ν_{17}	CH_2 antisymmetric stretch	3258.3	3164.9	3079.5	2968.9	2949	0.2	100.1	0.75	$91S_{17}$
	ν_{18}	*CH_2 twist	1437.6	1342.4	1319.3	1273.6	1275	0.1	18.6	0.75	$52S_{18}$, $36S_{19}$
	ν_{19}	CH_2 twist	1339.6	1264.2	1247.5	1199.8	1202	1.5	3.8	0.75	$31S_{19}$, $38S_{18}$, $30S_{20}$
	ν_{20}	*CH_2 rock	1216.1	1125.6	1110.6	1074.7	1084	0.9	0.4	0.75	$34S_{20}$, $37S_{21}$, $26S_{19}$
	ν_{21}	CH_2 rock	903.3	815.9	802.3	777.9	768	0.0	6.4	0.75	$54S_{21}$, $30S_{21}$
	ν_{22}	C≡C−H bend op	880.0	545.7	617.6	618.9	639	53.9	0.0	0.75	$101S_{22}$
	ν_{23}	C−C≡C bend op	432.4	307.4	365.4	341.9	334	1.5	12.6	0.75	$82S_{23}$, $17S_{24}$
	ν_{24}	torsion	117.6	113.6	112.9	115.7	109	3.5	2.3	0.75	$82S_{24}$, $18S_{23}$

[a] Vibrational frequencies are given in reciprocal centimeters. [b] Scale factors: 0.88 for C−H stretch, 0.9 for C−H bend and heavy atom stretch, 1.0 for heavy atom bend, C≡C stretch, and torsion, 1.3 for acetylene bends. [c] Infrared intensities are given in kilometers per mole; Raman activities are given in angstroms^4 per atomic mass unit. Both are from MP2/6-31G(d) calculations (unscaled), as are also potential energy distribution (PED) values.

torsional mode corresponding perhaps to the stronger sequence to higher frequencies and the weaker one to lower frequency involving the ν_{15} mode.

Next, there is some weak K structure between 140 and 150 cm^{-1} with an interval of about 1.5 cm^{-1}, which is more like that of a B-type band shown in Figure 12 of the *anti* conformer. This is assigned to ν_{15}, the in-plane skeletal bending mode of the anti form, in good agreement with the predicted frequency in Table 4. Although this mode could give an A/B hybrid band, there can be only a small A-type component. However, it should be noted that this band is only a small fraction of the intensity of the corresponding gauche band despite the ab initio dipole derivatives at the MP2 level indicating that it should be nearly half as strong as the gauche band.

The strong broad band around 110 cm^{-1} is assigned as the ν_{24} torsional mode of both conformers, in good agreement with the prediction by ab initio force constant calculations. But the torsional transitions can also be predicted from a torsional potential energy function derived from ab initio or hybrid DFT conformer energies in Table 3. These potential functions are given in Table 6 for each of the three methods used along with torsional kinetic constants calculated from the anti and gauche rotamer structures in a semirigid torsional model. These functions are shown in Figure 13 where the torsional angle is shifted by 180°. The torsional transitions are predicted at a little higher frequency than the observed values and with the gauche transitions higher than those for the anti form.

There are many detailed features on this band, around the peak but also on the low-frequency slope from 76 to 88 cm^{-1}. However, there are no particularly outstanding peaks that can easily be identified as central Q peaks. Such peaks would be expected if there were a strong band for the asymmetric torsional transitions of the anti conformer since it should give a pure C-type contour, but it has already been noted that the ν_{15} band of the anti form is also much weaker than predicted from ab initio dipole derivatives. Thus it appears that most of the intensity of this band is due to the gauche form and the ν_{24} gauche band could be a hybrid of A-, B-, and C-types, but in view of the observed band contour it must be mostly B-type with no outstanding central peaks.

Some peaks can be identified as torsional transitions of the gauche conformer as the structure on the low-frequency slope shows difference bands between the asymmetric torsion and the skeletal bending mode ν_{15}. Detailed analyses of these bands are given as a footnote to Table 6. A series of peaks at 116.57, 113.23 and 109.4 cm^{-1} have, thus, been assigned as consecutive torsional transitions of the gauche conformer. Sum bands of torsional intervals with the ν_{15} mode may also be present as structure on the low-frequency slope of the 334 cm^{-1} band. However, some of these features are more readily assigned as K structure of the anti conformer as there is extensive K structure on the high-frequency side of the 334 cm^{-1} peak having intervals between 1.4 and 1.28 cm^{-1}. The peak at 109.4 cm^{-1} is the strongest one in the band and two lower frequencies are further peaks, which have been assigned rather arbitrarily to the anti conformer as indicated in Table 6. There is a dip in the band around 102 cm^{-1} so that the peak at 103.1 appears to be perturbed to higher frequencies.

Conformational Stability

The determination of the conformational stability is rather difficult since many of the fundamentals for each conformer

TABLE 5: Vibrational Frequencies[a] of *gauche*-4-Fluoro-1-butyne

		RHF 6-31G unscaled	MP2 6-31G(d) unscaled	B3LYP 6-31G(d) unscaled	MP2 6-31G(d) scaled[b]	obs (gas)	IR int[c]	Raman act.[c]	dp ratios[d]	PED
ν_1	≡CH stretch	3676.2	3522.8	3495.9	3313.7	3333	52.0	30.4	0.19	$96S_1$
ν_2	*CH_2 symmetric stretch	3267.6	3119.2	3052.3	2926.1	2937	42.0	114.3	0.09	$95S_2$
ν_3	CH_2 symmetric stretch	3199.6	3101.0	3034.5	2909.0	2903	7.0	111.5	0.12	$94S_3$
ν_4	$C_1{\equiv}C_2$ stretch	2398.0	2173.1	2246.3	2152.8	2139	0.2	84.2	0.29	$83S_4$, $14S_{11}$
ν_5	*CH_2 scissors	1679.5	1581.9	1544.6	1501.5	1471	0.8	11.7	0.74	$99S_5$
ν_6	CH_2 scissors	1628.9	1526.2	1490.6	1448.2	1428	6.0	15.7	0.68	$98S_6$
ν_7	*CH_2 wag	1560.5	1470.5	1447.9	1395.3	1384	22.0	1.6	0.70	$90S_7$
ν_8	CH_2 wag	1525.6	1410.1	1386.3	1339.5	1338	6.2	13.0	0.51	$70S_8$, $12S_{18}$
ν_9	$C_3{-}C_4$ stretch	1156.8	1115.2	1098.4	1062.3	1053	41.5	7.7	0.74	$43S_9$, $21S_{21}$, $17S_{20}$
ν_{10}	CF stretch	1122.5	1061.1	1039.2	1015.9	1001	3.9	3.8	0.71	$18S_{10}$, $24S_{11}$, $17S_8$
ν_{11}	$C_2{-}C_3$ stretch	902.8	868.1	845.9	827.7	838	4.0	8.1	0.59	$50S_{11}$, $19S_{10}$, $15S_{20}$
ν_{12}	C≡C−H bend ip	895.1	585.5	626.2	639.5	643	48.4	7.4	0.09	$39S_{12}$, $20S_{15}$, $14S_{13}$
ν_{13}	skeletal bend	626.6	516.1	565.5	540.0	548	14.2	3.7	0.59	$14S_{13}$, $59S_{12}$, $19S_{15}$, $12S_{14}$
ν_{14}	CCF bend	392.5	358.0	371.1	363.6	374	1.8	5.7	0.72	$49S_{14}$, $14S_{13}$, $11S_{15}$
ν_{15}	skeletal bend ip	230.1	178.1	201.4	191.8	193	2.1	5.7	0.73	$17S_{15}$, $50S_{13}$, $20S_{24}$
ν_{16}	*CH_2 antisymmetric stretch	3332.7	3186.9	3105.0	2989.6	2980	37.2	60.8	0.74	$94S_{16}$
ν_{17}	CH_2 antisymmetric stretch	3245.7	3155.1	3072.8	2959.8	2974	6.4	112.9	0.50	$93S_{17}$
ν_{18}	*CH_2 twist	1401.5	1309.7	1291.7	1245.6	1260	1.8	16.0	0.64	$49S_{18}$, $30S_{19}$
ν_{19}	CH_2 twist	1353.8	1272.4	1256.9	1208.6	1217	2.5	6.9	0.74	$49S_{19}$, $29S_{18}$, $15S_{20}$
ν_{20}	*CH_2 rock	1205.0	1140.5	1109.0	1088.2	1077	27.1	4.2	0.32	$29S_{20}$, $28S_9$, $26S_{10}$
ν_{21}	CH_2 rock	948.8	893.9	878.1	858.5	853	14.3	7.3	0.58	$45S_{21}$, $21S_9$, $15S_{10}$
ν_{22}	C≡C−H bend op	885.8	538.5	607.4	610.5	639	48.9	4.2	0.69	$95S_{22}$
ν_{23}	C−C≡C bend op	415.5	296.3	349.1	326.9	325	1.0	10.8	0.74	$68S_{23}$, $16S_{24}$
ν_{24}	torsion	117.1	110.8	110.9	113.6	117	2.1	2.8	0.74	$54S_{24}$, $17S_{15}$, $15S_{13}$

[a] Vibrational frequencies are given in reciprocal centimeters. [b] Scale factors: 0.88 for C−H stretch, 0.9 for C−H bend and heavy atom stretch, 1.0 for heavy atom bend, C≡C stretch, and torsion, and 1.3 for acetylene bends. [c] Infrared intensities are given in kilometers per mole; Raman activities are given in angstroms^4 per atomic mass unit from MP2/6-31G(d) calculations. [d] Calculated value.

are predicted to be near coincident. However, a comparison of the Raman data in the liquid phase to that in the solid clearly shows several low-frequency lines disappearing from the spectrum of the liquid with solidification of the sample. The most noteworthy line is the one at 491 cm^{-1}, which is a pronounced line but is absent in the spectrum of the solid. Only the anti conformer is predicted to have a fundamental in this spectral region. The closest predicted gauche lines are 127 cm^{-1} lower (ν_{13} predicted at 364 cm^{-1}) or 49 cm^{-1} higher (ν_{13} predicted at 540 cm^{-1}) in frequency, where these modes for the gauche conformer are observed at 373 and 558 cm^{-1}, respectively. Additional anti bands that disappear from the Raman spectrum of the liquid are found at 167, 382, and 954 cm^{-1}. The 954 cm^{-1} line is also important since there is no gauche fundamental predicted in the 900−1000 cm^{-1} region, so these data clearly show that the gauche conformer remains in the solid state.

To determine the conformational stability in the xenon solution, two pairs of bands at 488 (anti)/548 (gauche) and 848 (anti)/953 (gauche) cm^{-1} were used to determine the enthalpy difference between the conformers. From these spectral data for the low-frequency pair (Figure 3) it is obvious that the increase in the intensity of the infrared band assigned to the anti conformer as the temperature decreases confirms the stability of the anti conformer over the gauche rotamer in the xenon solution. To obtain the enthalpy difference, spectral data at 10 different temperatures were obtained from these bands over the temperature range from −55 to −100 °C (Table 7). The intensities of the conformer pairs were fit to the equation $-\ln K = (\Delta H/RT) - (\Delta S/R)$, where K is the intensity ratio (I_a/I_g) and it is assumed that ΔH is not a function of temperature. From a least-squares fit and the slope of the line, an average ΔH value of 215 ± 22 cm^{-1} (2.57 ± 0.26 kJ/mol) was obtained from these two conformer pairs. Similar data were also collected for these two pairs of bands (Figures 13 and 14) for a krypton solution over the temperature range −110 to −135 °C at six different temperatures. A least-squares fit of these data gave an average ΔH value of 170 ± 17 cm^{-1}, again with the anti conformer the more stable rotamer. This conformer stability is consistent with the ab initio predictions where the anti conformer is estimated to be more stable with values in the range of 427 to 245 cm^{-1}.

Asymmetric Torsional Potential

As indicated earlier, there are several observed asymmetric torsional transitions for both anti and gauche conformers. The torsional fundamental for the anti conformer is assigned at 109.40 cm^{-1} and that for the gauche rotamer at 116.57 cm^{-1}. Additional excited-state torsional transitions fall to lower frequency for both rotors. With these assignments, a potential function governing internal rotation has been calculated. The torsional potential is represented by a Fourier cosine series in the internal rotation angle ϕ:

$$V(\phi) = \sum_{i=1}^{6} \left(\frac{V_i}{2}\right)(1 - \cos i\,\phi)$$

where ϕ and i are the torsional angle and foldness of the barrier, respectively. It is assumed that V_5 and V_6 are relatively small and they are not included in the series. The potential parameters V_1, V_2, V_3, and V_4 were calculated from the input of the frequencies for the two torsional transitions, the experimental ΔH value from the xenon solution, the gauche dihedral angle, and the internal rotation constant $F(\phi)$. The internal rotation constant also varies as a function of the internal rotation angle,

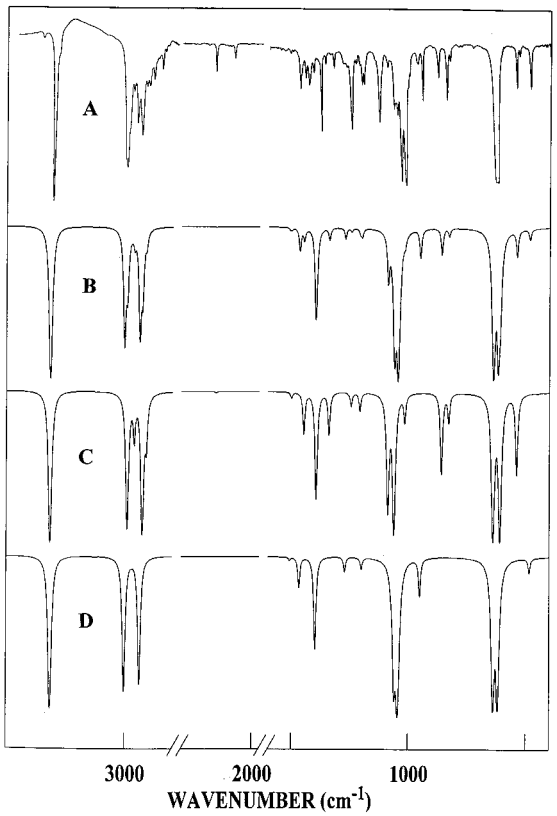

Figure 9. Comparison of experimental and calculated infrared spectra of 4-fluoro-1-butyne: (A) observed infrared spectrum of 4-fluoro-1-butyne in liquid xenon; (B) simulated infrared spectrum of mixture of trans and gauche conformers; (C) simulated infrared spectrum of pure gauche conformer; and (D) simulated infrared spectrum of pure anti conformer.

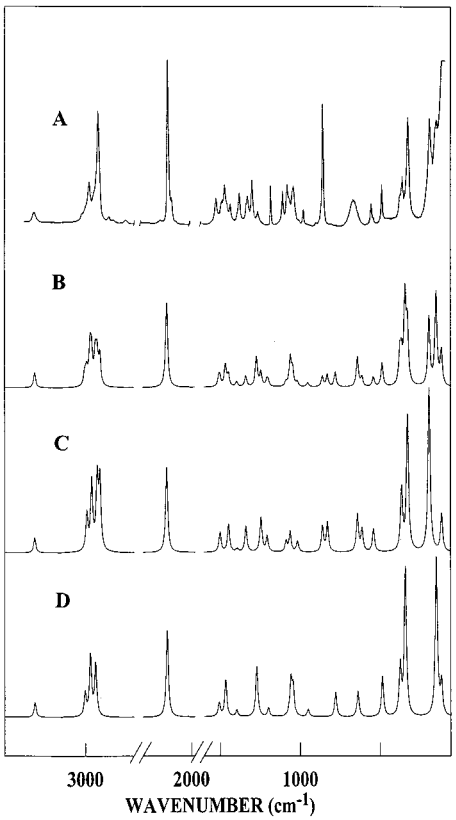

Figure 10. Comparison of experimental and calculated Raman spectra of 4-fluoro-1-butyne: (A) observed Raman spectrum of 4-fluoro-1-butyne in liquid phase; (B) simulated Raman spectrum of mixture of trans and gauche conformer; (C) simulated Raman spectrum of pure gauche conformer, and (D) simulated Raman spectrum of pure anti conformer.

and this is approximated by another Fourier series:

$$F(\phi) = F_0 + \sum_{i=1}^{6} F_i \cos \phi$$

The relaxation of the structural parameters, $B(\phi)$, during the internal rotation can be incorporated into the above equation by assuming them to be small periodic functions of the torsional angle of the general type

$$B(\phi) = a + b \cos \phi + c \sin \phi$$

The series approximating the internal rotation constants (Table 6) for 4-fluoro-1-butyne was determined by use of structural parameters from the MP2/6-31G(d) ab initio calculations. In the initial calculation of the potential parameters, the fundamental torsional transitions for the two conformers (Table 6) were used along with the value 215 cm^{-1} for ΔH and a dihedral angle of 62.66° for the gauche rotamer. As the values for the potential parameters converged, four more transitions for the anti rotamer were added to the calculation and then two additional transitions of the gauche form. The final resulting values for the potential parameters are listed in Table 6 and the potential function is shown in Figure 15.

Discussion

The conformational stability determined from the xenon solution, with the anti conformer more stable by 215 ± 22 cm^{-1} (2.57± 0.26 kJ/mol), is expected to be close to the value in the gas phase.[26−30] This value is in good agreement with the predicted values ranging from 274 cm^{-1} [MP2/6-311+G(2df,-2p)] to 362 cm^{-1} [B3LYP/6-31G(d)] excluding the Hartree−

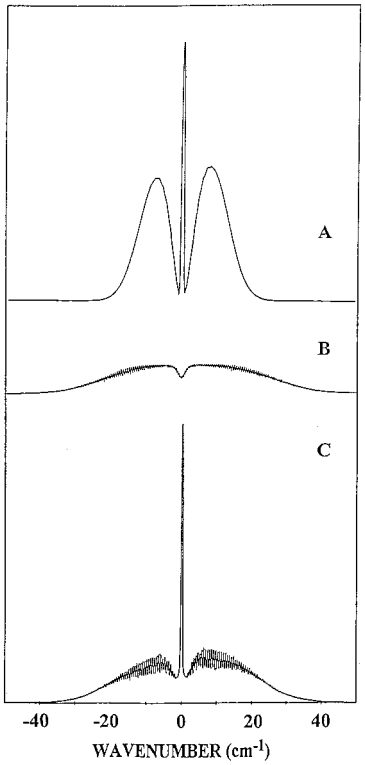

Figure 11. Pure (A) type A, (B) type B, and (C) type C infrared contours for gauche conformer of 4-fluoro-1-butyne.

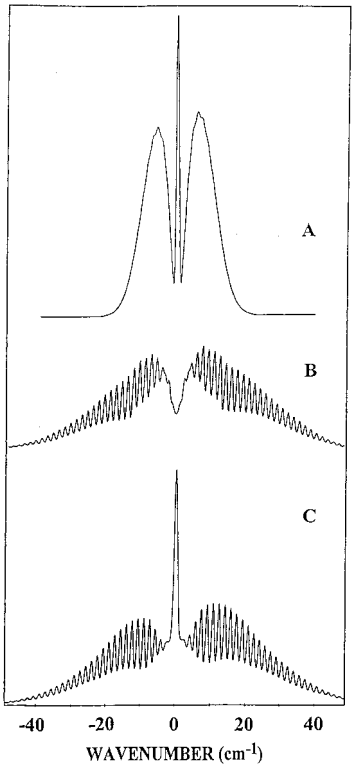

Figure 12. Pure (A) type A, (B) type B, and (C) type C infrared contours for anti conformer of 4-fluoro-1-butyne.

TABLE 6: Potential Constants, Kinetic Constants,[a] and Torsional Transitions for the Asymmetric Torsion on 4-Fluoro-1-butyne

	RHF 6-31G	MP2 6-31G(d)	B3LYP 6-31G(d)	obs[b] far IR	exptl[c]
V_1	1149.7	642.9	759.8		438 ± 14
V_2	−220.7	−158.9	−189.2		−157 ± 12
V_3	1478.5	1561.2	1392.0		1137 ± 5
V_4	−38.2	−68.2	19.5		17 ± 6
V_5	−21.2	−18.7	−63.1		
torsional transitions[d]					
anti	1 ← 0		116.5	109.40	110.68
	2 ← 1		114.2	107.38	107.55
	3 ← 2		111.7	105.20	104.28
	4 ← 3		109.1	103.10	100.86
	5 ← 4		106.4	97.91	97.26
gauche	1± ← 0±		133.9	116.57	116.81
	2± ← 1±		130.0	113.23	113.41
	3± ← 2±		125.9	109.40	109.76
ΔH	0± ← 0			215 ± 22	215 ± 31

[a] $F_0 = 1.456\ 25$, $F_1 = -0.381\ 39$, $F_2 = 0.226\ 45$, $F_3 = -0.068\ 85$, $F_4 = 0.028\ 02$, $F_5 = -0.009\ 73$, $F_6 = 0.003\ 80$, and $F_7 = -0.001\ 51$ cm^{-1}. [b] Note confirmation of gauche assignments from difference bands: 116.57 ≈ 192.58 − 76.19; 113.23 ≈ 192.58 − 78.58; 109.4 ≈ 192.58 − 83.20 cm^{-1}. Also there is evidence of sum bands: 308.7 ≈ 192.58 + 116.57; 306.2 ≈ 192.58 + 113.23 cm^{-1}, but these are more probably K structure of the anti band at 326 cm^{-1}. [c] Potential constants obtained from fit of the torsional transitions, ΔH, and dihedral angle. [d] Torsional transitions are given in reciprocal centimeters.

Fock calculations. However, it should be noted that this result is somewhat surprising since 1-fluoropropane has the gauche conformer as the more stable rotamer by 99 ± 5 cm^{-1} (1.16 ± 0.06 kJ/mol) from variable temperature Fourier transform infrared spectral studies of a xenon solution.[17] This experimental result for 1-fluoropropane is consistent with the ab initio predicted energy difference of 112 cm^{-1} obtained from MP2/6-311+G(d,p) calculations. The difference in these two molecules (YCH_2CH_2F) is the substitution of an acetylenic group as Y for the methyl group. This difference in Y results in the C_3–C_4 bond distance to be predicted to be about 0.010 Å shorter in 1-fluoropropane than the corresponding bond distance in 4-fluoro-1-butyne. Undoubtedly this C_3–C_4 bond distance is an important factor in determining the conformational stability of YCH_2CH_2F molecules.

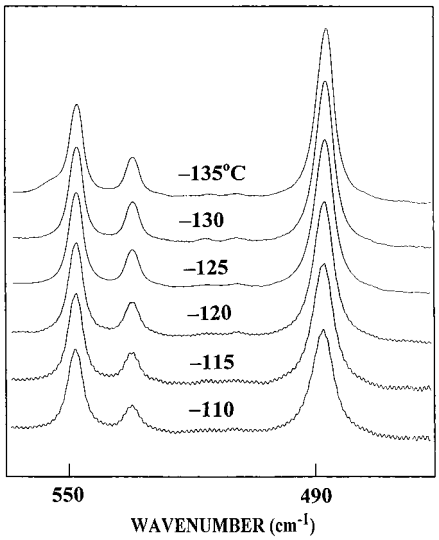

Figure 13. Temperature-dependent infrared spectrum (460−570 cm^{-1}) of 4-fluoro-1-butyne in liquid krypton.

TABLE 7: Temperature and Intensity Ratios from Conformational Study of 4-Fluoro-1-butyne

T (°C)	1000/T (K)	I_{488}/I_{548}	I_{953}/I_{848}
−55	4.58	0.862	0.520
−60	4.69	1.005	0.574
−65	4.80	1.101	0.609
−70	4.92	1.172	0.601
−75	5.05	1.207	0.641
−80	5.18	1.263	0.646
−85	5.31	1.278	0.661
−90	5.46	1.362	0.669
−95	5.61	1.402	0.687
−100	5.78	1.416	0.764
ΔH^a (cm^{-1})		255 ± 35	174 ± 20

[a] Average value of ΔH is 215 ± 22 cm^{-1} (2.52 ± 0.25 kJ/mol) with the anti conformer, which is the more stable form.

TABLE 8: Temperature and Intensity Ratios from Conformational Study of 4-Fluoro-1-butyne in Krypton Solution

T (°C)	1000/T (K)	I_{488}/I_{548}	I_{953}/I_{848}
110	6.135	1.683	0.816
115	6.329	1.772	0.840
120	6.536	1.960	0.890
125	6.757	2.102	0.947
130	6.993	2.219	0.964
135	7.246	2.326	0.994
ΔH^a (cm^{-1})		210 ± 17	130 ± 13

[a] Average value of ΔH is 170 ± 17 cm^{-1} (2.04 ± 0.02 kJ/mol) with the anti conformer, which is the more stable form.

The change from the anti conformer being the stable form in the vapor to the gauche conformer being the stable form in the solid probably arises from the fact that the gauche conformer is predicted to have a dipole moment of 2.12 D, whereas the anti form is predicted to have a dipole moment of 1.61,D. The larger dipole moment for the gauche conformer will make more of this conformer present in the liquid phase compared to the amount in the vapor. However, the packing factor in the

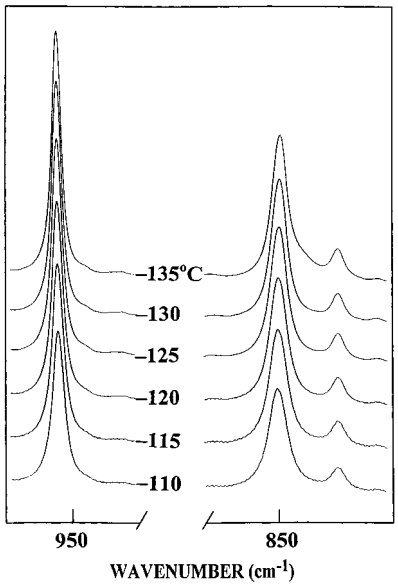

Figure 14. Temperature-dependent infrared spectrum (800−990 cm^{-1}) of 4-fluoro-1-butyne in liquid krypton.

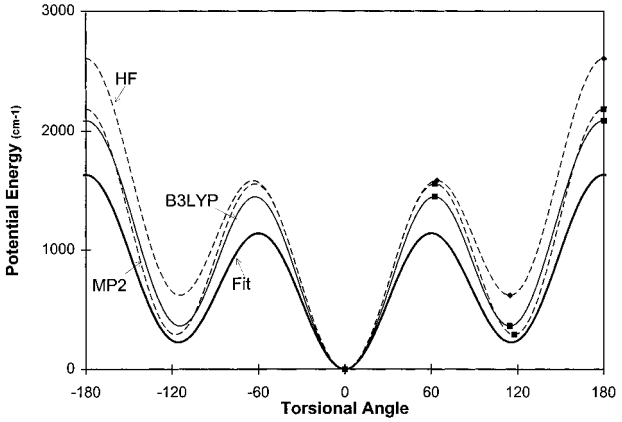

Figure 15. Asymmetric torsional potential functions of 4-fluoro-1-butyne as determined by *ab initio* calculations with RHF/6-31G, MP/6-31G(d), and B3LYP/6-31G(d).

crystalline solid is expected to be the dominant factor in determining which conformer remains in the solid.

The heavy atom distances are predicted to be essentially the same for the two conformers, except that the C−F distance is predicted to be 0.0032 Å longer for the anti conformer compared to the similar distance for the gauche form. The $C_2C_3C_4$ and C_3C_4F angles are predicted to be 1.3° and 1.2° larger, respectively, for the gauche conformer compared to those for the anti form. Since the structural parameters are nearly the same for the two conformers, the corresponding force constants for the two conformers are also predicted to be nearly the same.

For fluoro- and hydrocarbon compounds one can usually predict the frequencies of the fundamentals from MP2/6-31G(d) calculations by utilizing only two scaling factors of 0.88 for the carbon−hydrogen stretches and 0.9 for the carbon−hydrogen bends and heavy atom stretches while keeping the other force constants with the predicted values. Such predictions usually give fundamental frequencies with average errors of 10−12 cm^{-1}. However, for the acetylene group the C≡C stretch is not scaled and the C≡C−H and C−C≡C bends need to be scaled by a factor of 1.3 to give reasonable results from the MP2/6-31G(d) calculations. By use of these three scaling factors, the fundamentals frequencies are predicted with errors of 1.2% (10 cm^{-1}) for the gauche conformer and 1.3% (12 cm^{-1}) for the anti conformer. It should be noted that B3LYP/6-31G(d) calculations predict the fundamentals within 1.3% (11 cm^{-1}) for the gauche conformer and 1.4% (14 cm^{-1}) for the anti conformer without any scaling factors.

The potential energy distributions are relatively pure for the anti conformer, with significant mixing only for the $C_2C_3C_4$ bend (ν_{13}), the CH_2 twist, and the $*CH_2$ rock. However, for the gauche conformer the mixing is quite extensive among the modes below 1000 cm^{-1} except for the C≡C−H and C−C≡C out-of-plane bends. Many of these modes have PEDs, which have less than 40% from any one symmetry coordinate. Although the descriptions of the vibrations for the two conformers have been keep the same, it is obvious that many of those in the same frequency region for the gauche conformer differ significantly from those for the anti conformer. For some, like the C−F stretch, there is no one band that can be described as mainly due to this motion for the gauche conformer.

The potential parameters obtained from the fit of the torsional data has a V_3 term of 1137 ± 5 cm^{-1}, which is about 250 cm^{-1} lower than the value of this parameter from the B3LYP/6-31G(d) calculation and more than 400 cm^{-1} lower than the similar parameter from the MP2/6-31G(d) calculation. We have frequently found the parameters obtained from the fitting of the torsional data to be somewhat smaller than those predicted from ab initio calculations. The other parameters, i.e., V_1, V_2,and V_4, obtained from the B3LYP/6-31G(d) calculation are in reasonable agreement with the experimentally determined values. In Figure 13 the various potential functions obtained from the ab initio calculations are compared to that obtained experimentally. The experimental function has an anti to gauche barrier of 1142 cm^{-1}, a gauche to anti barrier of 931 cm^{-1}, and a gauche to gauche barrier of 1364 cm^{-1}. All of these barrier values are significantly lower than the predicted values.

With the ΔH value of 215 ± 22 cm^{-1}, the abundance of the gauche conformer is predicted to be 42% at ambient temperature, so it should be possible to obtain microwave spectra of both conformers. It would be of interest to obtain such data for structural determinations so the parameters could be compared to the corresponding ones for the 1-fluoropropane molecule as well as compare them to the ab initio predicted values. Alternatively, electron diffraction data could be used for this purpose. These data could then be used to verify that the relative C_3–C_4 bond distance is the major factor determining the conformational stability of YCH_2CH_2F molecules.

Acknowledgment. J.R.D. acknowledges partial support of these studies by the University of Missouri−Kansas City Faculty Research Grant program.

Supporting Information Available: Table 1S, listing observed infrared and Raman wavenumbers (cm^{-1}) for 4-fluoro-1-butyne, and Table 2S, listing symmetry coordinates for vibrations of 4-fluoro-1-butyne. This material is available free of charge via the Internet at http://pubs.acs.org.

References and Notes

(1) Durig, J. R.; Liu, J.; Little, T. S. *J. Chem. Phys.* **1991**, *95*, 4664.
(2) Durig, J. R.; Liu, J.; Little, T. S. *J. Mol. Struct.* **1991**, *248*, 25.
(3) El-Bermani, H. F.; Jonathan, N. *J. Chem. Phys.* **1968**, *49*, 340.
(4) Woodward, J.; El-Bermani, H. F.; Jonathan, N. *J. Am. Chem. Soc.* **1970**, *92*, 6750.
(5) Mukhtarov, A.; Mukhtarov, E. I.; Akhunova, L. A. *Zh. Strukt. Khim.* **1966**, *7*, 607.
(6) Mukhtarov, A. *Izv. An. SSSR Fiz.* **1958**, *22*, 1154.
(7) Mukhtarov, A. *Izv. An. Azerb. SSSR Fiz.* **1964**, *6*, 37.

(8) Mukhtarov, A.; Mukhtarov, E. I. *Zh. Fiz. Khim*. **1968**, *42*, 2025.
(9) Pruettiangkura, P.; Gupta, A.; Schwartz, M. *J. Fluorine Chem*. **1981**, *17*, 155.
(10) Musbally, G. M.; Aleman, H.; Lielmezs, J. *Thermochim. Acta* **1972**, *3*, 327.
(11) Lere-Porte, J. P.; Petrissans, J. *J. Mol. Struct*. **1976**, *34*, 55.
(12) Huang, J.; Hedberg, K. *J. Am. Chem. Soc*. **1990**, *112*, 2070.
(13) Kueseth, K. *Acta Chem. Scand*. **1974**, *A28*, 482.
(14) Kueseth, K. *Acta Chem. Scand*. **1978**, *A32*, 63.
(15) Durig, J. R.; Hester, R. R.; Robb, J. B., II *J. Mol. Struct.* 2000, in press.
(16) Durig, J. R.; Godbey, S. E.; Sullivan, J. F. *J. Chem. Phys.* **1984**, *80*, 5983.
(17) Guirgis, G. A.; Zhu, X.; Durig, J. R. *Struct. Chem*. **1999**, *10*, 445.
(18) Frisch, M. J.; Trucks, G. W.; Schlegel, H. B.; Gill, P. M. W.; Johnson, B. G.; Robb, M. A.; Cheeseman, J. R.; Keith, T. A.; Petersson, G. A.; Montgomery, J. A.; Raghavachari, K.; Al-Laham, M. A.; Zakrzewski, V. G.; Ortiz, J. V.; Foresman, J. B.; Cioslowski, J.; Stefanov, B. B.; Nanayakkara, A.; Challacombe, M.; Peng, C. Y.; Ayala, P. Y.; Chen, W.; Wong, M. W.; Andres, J. L.; Replogle, E. S.; Gomperts, R.; Martin, R. L.; Fox, D. J.; Binkley, J. S.; Defrees, D. J.; Baker, J.; Stewart, J. P.; Head-Gordon, M.; Gonzalez, C.; Pople, J. A. *Gaussian 94 (Revision B.3)*, Gaussian Inc., Pittsburgh, PA, 1995.
(19) Pulay, P. *Mol. Phys*. **1969**, *17*, 197.
(20) Guirgis, G. A.; Durig, J. R.; Bell, S. *J. Mol. Struct*. **1989**, *196*, 101.
(21) Guirgis, G. A.; Zhu, X.; Yu, Z.; Durig, J. R. *J. Phys. Chem*. 2000, *104*, 4383.
(22) Frisch, M. J.; Yamagushi, Y.; Gaw, J. F.; Schaefer, H. F., III; Binkley, J. S. *J. Chem. Phys.* **1986**, *84*, 531.
(23) Amos, R. D. *Chem. Phys. Lett.* **1986**, *124*, 376.
(24) Polavarapu, P. L. *J. Phys. Chem.* **1990**, *94*, 8106.
(25) Chantry, G. W. In *The Raman Effect*; Anderson, A., Ed.; Marcel Dekker Inc.: New York, 1971; Vol. 1, Chapt. 2.
(26) Herrebout, W. A.; van der Veken B. J. *J. Phys. Chem*. **1996**, *100*, 9671.
(27) Herrebout, W. A.; van der Veken, B. J.; Wang, A.; Durig, J. R. *J. Phys. Chem*. **1995**, *99*, 578.
(28) van der Veken, B. J.; DeMunck, F. R. *J. Chem. Phys*. **1992**, *97*, 3060.
(29) Bulanin, M. O. *J. Mol. Struct.* **1973**, *19*, 59.
(30) Bulanin, M. O. *J. Mol. Struct.* **1995**, *347*, 73.